Electronic Supplementary Material (ESI) for Physical Chemistry Chemical Physics.

Electronic Supplementary Information

Experimental Quantification of the Electron Spectral-Diffusion under Static DNP conditions

Krishnendu Kundu, Marie Ramirez Cohen, Akiva Feintuch, Daniella Goldfarb and Shimon Vega

Department of Chemical and Biological Physics, Weizmann Institute of Science, Rehovot, Israel

1. The T_{1e} as a function of various position of the EPRline of TEMPOL

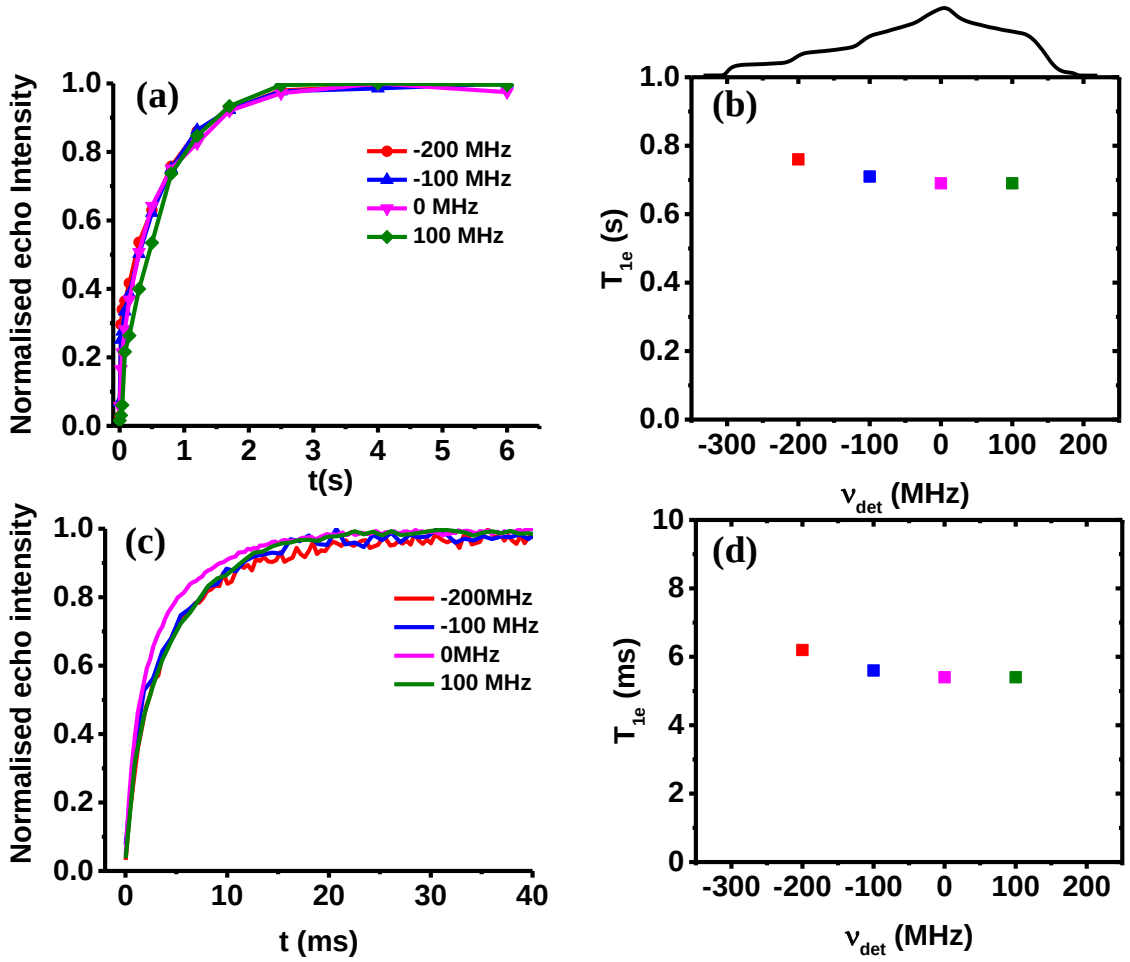

Figure S1. Saturation recovery signal recorded with the sample III[40] at four different places on the EPR line of at 3K (a) and 20K (c). The slowest component (major contribution) resulted from the bi-exponential fitting of the signal have been shown in (b) for 3K and (d) for 20K as a function of position on the EPR line.

2. Comparison of ELDOR spectra of sample sets I and II

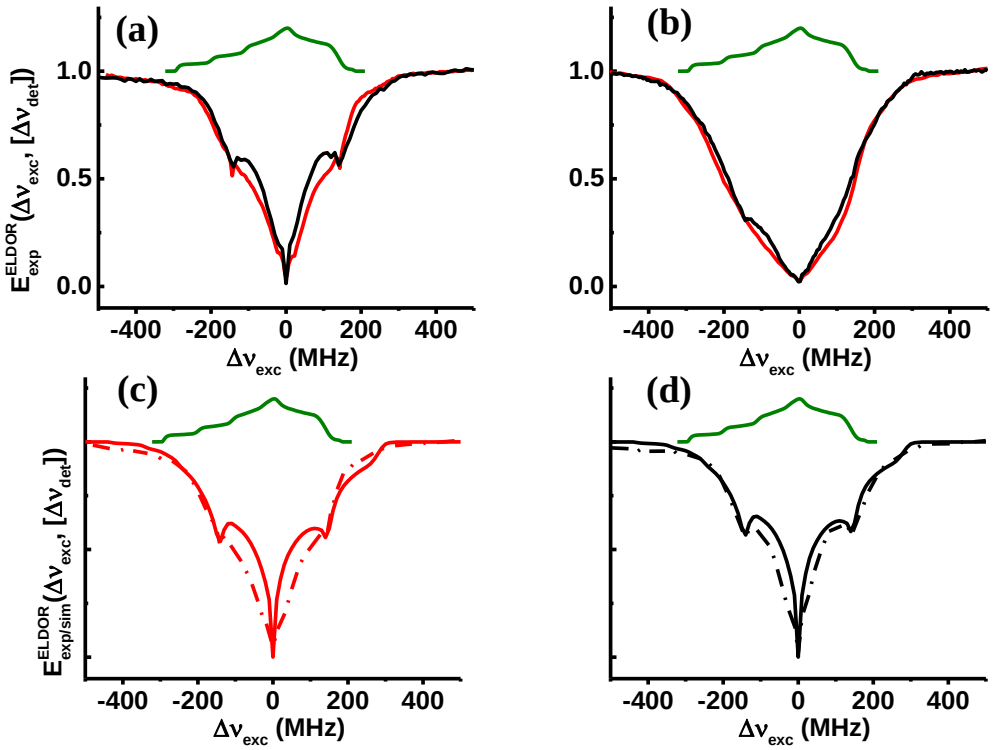

Figure S2. A comparison between the experimental steady-state ELDOR spectra of samples I^{20} (red) and II^{20} (black) in (a) and of samples I^{40} (red) and II^{40} (black) in (b). These experiments were conducted at 20 K and with a MW irradiation time $t_{MW} = 20ms$. Simulated ELDOR spectra are shown as solid lined in (c) with $\Lambda^{\mathrm{eSD}} = 500\mu\mathrm{s}^{-3}$ and $A^{\mathrm{SE}} = 4.5\mathrm{MHz}$ in (d) with $\Lambda^{\mathrm{eSD}} = 400\mu\mathrm{s}^{-3}$ and $A^{\mathrm{SE}} = 4\mathrm{MHz}$. All other simulation parameters are tabulated in Table 1. The dotted lines are the experimental ELDOR spectra copied from (a) of I^{20} in (c) and of II^{20} in (d). Notice that the ^{14}N-SE features in the spectra are not taken into account during the simulations.

3. Evaluation of the error in Λ^{eSD} for fits of sample set II

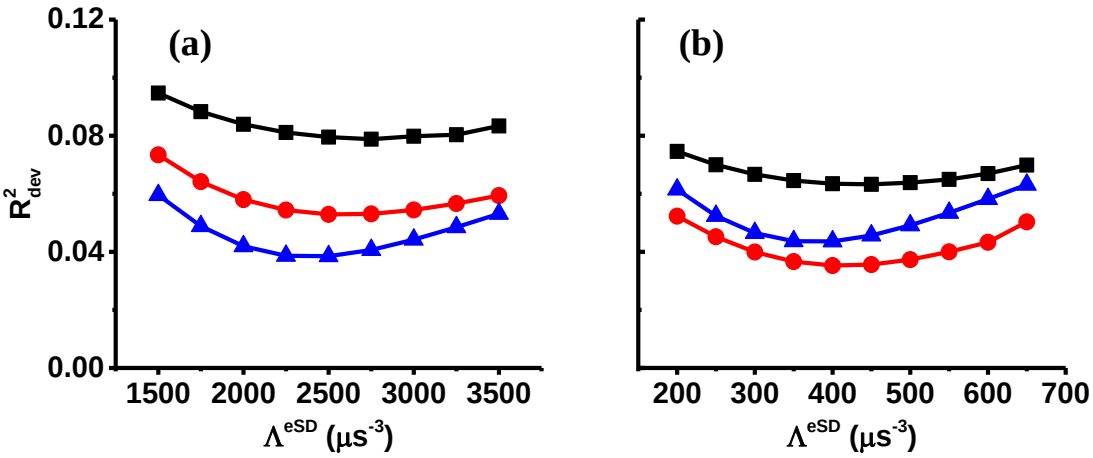

Figure S3: The R^2_{dev} values of the best fit simulation procedure for determining Λ^{eSD} are shown for samples II^{40} and II^{20} recorded at 20 K at the EPR spectrometer. The sum of the squares of the deviations, R^2_{dev}, between the experimental ELDOR recorded at 20 K, $E^{ELDOR}_{exp}(\Delta\nu_{exc},[\Delta\nu_{det}])$ and simulated ELDOR, $E^{ELDOR}_{sim}(\Delta\nu_{exc},[\Delta\nu_{det}])$ as a function of $\Delta\nu_{exc}$ are calculated for varying Λ^{eSD} for sample II^{40} in (a) and sample II^{20} in (b). The other simulation parameters are tabulated in Table 1.

4. **Time dependent experiments**

Table S1: The depolarization decay times τ_{dep} during MW irradiation of sample II^{40} at 10 K.
The frequency values $\Delta\nu_{\mathrm{det}}$ and $\Delta\nu_{exc}$ of four depolarization experiments are listed and the decay times obtained from analyzing the initial time dependence of the four ELDOR signals reported. Relying on the best fit parameter $\Lambda^{eSD} = 2500\ \mu s^{-3}$ the simulated decay times are shown to be similar to experimental results.

$\Delta\nu_{\mathrm{det}}$ (MHz)	$\Delta\nu_{\mathrm{exc}}$ (MHz)	τ_{dep} (EXP)	τ_{dep} (SIM)
0	-100	1.1 ms	1.7 ms
0	100	1.5 ms	1.7 ms
100	0	0.7 ms	0.9 ms
100	-200	3.4 ms	5.1 ms

Table S2: The depolarization decay times τ_{dep} during MW irradiation of sample II^{20} at 10 K.
The frequency values $\Delta\nu_{\mathrm{det}}$ and $\Delta\nu_{exc}$ of four depolarization experiments are listed and the decay times obtained from analyzing the initial time dependence of the four ELDOR signals reported. Relying on the best fit parameter $\Lambda^{eSD} = 400\ \mu s^{-3}$ the simulated decay times are shown to be similar to experimental results.

$\Delta\nu_{\mathrm{det}}$ (MHz)	$\Delta\nu_{\mathrm{exc}}$ (MHz)	τ_{dep} (EXP)	τ_{dep} (SIM)
0	-100	5.4 ms	5.9 ms
0	100	5.5 ms	5.4 ms
100	0	4.2 ms	4.8 ms
100	-200	9.6 ms	9.5 ms

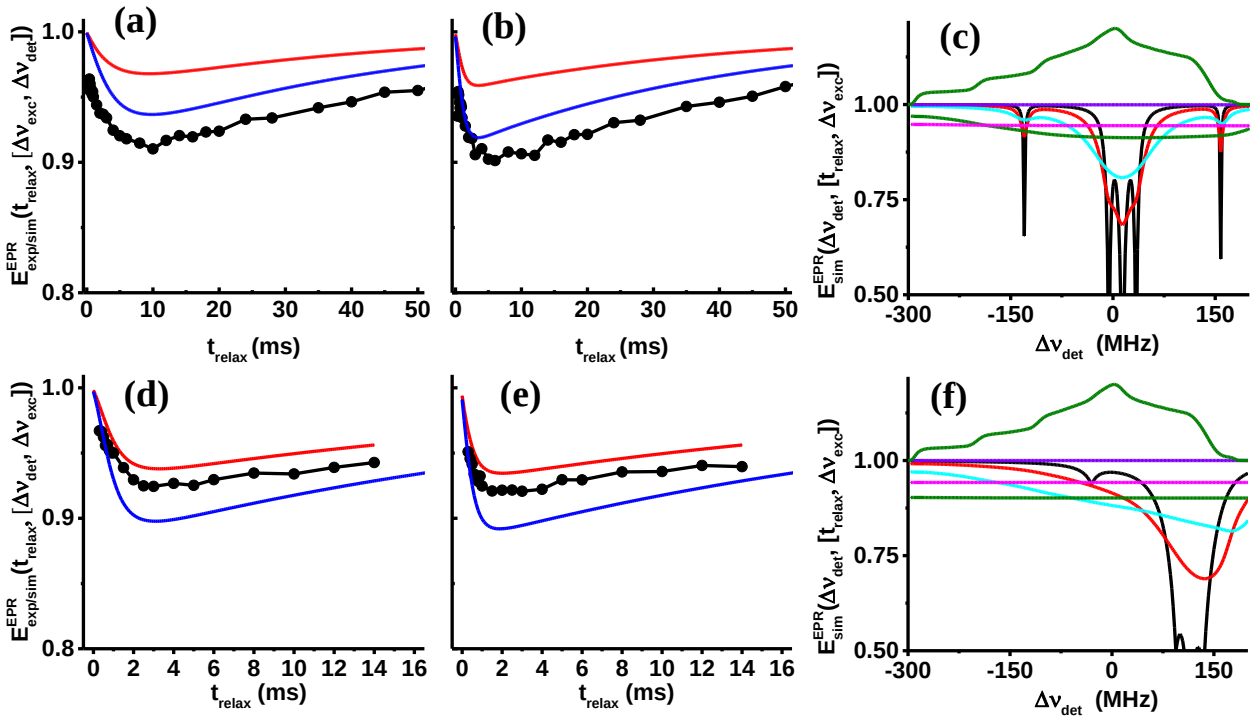

Figure S4: In (a) and (b) normalized EPR line intensities of the sample II[20], measured and simulated as a function of the delay time t_{relax} between a $t_{MW} = 100\,\mu s$ MW excitation and the echo signal detection (see Fig. 1a), are shown. The frequencies $\Delta\nu_{det}$ and $\Delta\nu_{exc}$ of the EPR data are in (a) $\Delta\nu_{det} = -200\,MHz$ and $\Delta\nu_{exc} = 0\,MHz$ in (b) $\Delta\nu_{det} = -100\,MHz$ and $\Delta\nu_{exc} = 0\,MHz$. The black dots are derived from the experimental EPR spectra in Fig. 6a. The red lines correspond to the simulated EPR spectra in Fig. 6b. The results in (a) and (b) show a 0.05 deviation, which could be a result of the fact that during the simulations no ^{14}N-SE effects were taken into account. To demonstrate the influence of local ^{14}N-SE induced depolarizations of the EPR intensities, we show in (c) EPR spectra that were simulated considering such depolarization effects. This was done by adding to the simulations of the spectra in Fig. 6b effective SE irradiations at $\Delta\nu_{exc} = \pm 20$ MHZ with a ^{14}N-SE parameter $A^{SE}_{^{14}N} = 0.8$ MHz [1]. The t_{relax} dependent intensities corresponding to these simulations are plotted in blue in (a) and (b).

Similarly, in (d) and (e) normalized EPR line intensities of the sample II[40], measured and simulated as a function of the delay time t_{relax} between a $t_{MW} = 100\,\mu s$ MW excitation and the echo signal detection (see Fig. 1a), are shown. The frequencies $\Delta\nu_{det}$ and $\Delta\nu_{exc}$ of the EPR data are in (d) $\Delta\nu_{det} = -200\,MHz$ and $\Delta\nu_{exc} = 100\,MHz$ in (e) $\Delta\nu_{det} = -100\,MHz$ and ; $\Delta\nu_{exc} = 100\,MHz$. On this sample no full EPR spectra were recorded. The red lines correspond to EPR intensities simulated without considering ^{14}N-SE effects. EPR spectra with the effective ^{14}N-SE irradiation present are shown in (f). The blue lines in (d) and (e) are derived from these spectra.

Table S3: The decay time constant τ_{decay} of the initial decay shown in figure S3 of sample II^{40} at 10 K.

The frequency values $\Delta\nu_{\mathrm{det}}$ and $\Delta\nu_{exc}$ of two experiments are listed and the decay times called here τ_{decay} obtained from analyzing the time dependence of the two ELDOR signals reported. Relying on the best fit parameter $\Lambda^{eSD} = 2500\ \mu s^{-3}$ the simulated decay times are shown to be similar to experimental results.

$\Delta\nu_{\mathrm{det}}$ (MHz)	$\Delta\nu_{\mathrm{exc}}$ (MHz)	τ_{decay} (EXP)	τ_{decay} (SIM)
-200	100	1.1 ms	1.1 ms
-100	100	0.4 ms	0.5 ms

Table S4: The decay time constant τ_{decay} of the initial decay shown in figure S3of sample II^{20} at 10 K.

The frequency values $\Delta\nu_{\mathrm{det}}$ and $\Delta\nu_{exc}$ of two repolarization experiments are listed and the recovery times called here τ_{delay} obtained from analyzing the time dependence of the two ELDOR signals reported. Relying on the best fit parameter $\Lambda^{eSD} = 400\ \mu s^{-3}$ the simulated decay times are shown to be similar to experimental results.

$\Delta\nu_{\mathrm{det}}$ (MHz)	$\Delta\nu_{\mathrm{exc}}$ (MHz)	τ_{decay} (EXP)	τ_{decay} (SIM)
-200	0	3.0 ms	3.0 ms
-100	0	1.3 ms	1.1 ms

5. **Concentration dependent experiments**

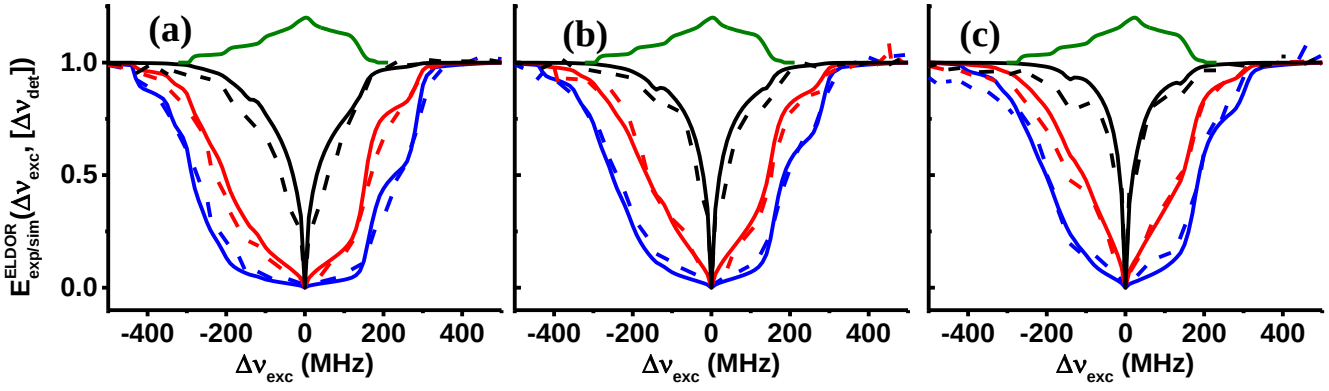

Figure S5: Temperature and concentration dependence of ELDOR spectra of the samples III [25–35] recorded at the DNP spectrometer Temperature dependence of experimental (dotted lines) and simulated (solid lines) steady-state $E^{ELDOR}_{exp/sim}(\Delta\nu_{exc},[\Delta\nu_{det}])$ spectra of four samples III [35] in (a), III [30] in (b) and III [25] in (c) recorded with $\Delta\nu_{det}=0\,MHz$ at the DNP spectrometer. The spectra were collected at 5 K (in blue), 10 K (in red) and

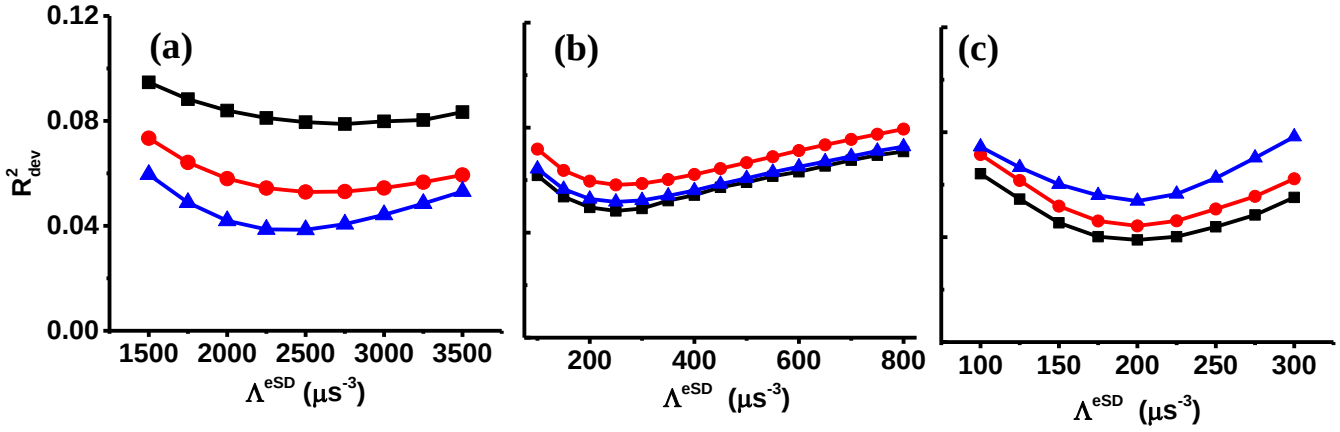

Figure S6: The R^2_{dev} values of the best fit simulation procedure for determining Λ^{eSD} are shown for samples II [40] and II [20] recorded at 20 K at the EPR spectrometer. The sum of the squares of the deviations, R^2_{dev}, between the experimental ELDOR recorded at 20 K, $E^{ELDOR}_{exp}(\Delta\nu_{exc},[\Delta\nu_{det}])$ and simulated ELDOR, $E^{ELDOR}_{sim}(\Delta\nu_{exc},[\Delta\nu_{det}])$ as a function of $\Delta\nu_{exc}$ are calculated for varying Λ^{eSD} for sample III [35] in (a), sample III [30] in (b) and sample III [25] in (c). The other simulation parameters are tabulated in Table 2. The detection frequency of the ELDOR spectra were set at $\nu_{det}=-100\,MHz$ (in black), $\nu_{det}=0\,MHz$ (in red), $\nu_{det}=100\,MHz$ (in blue).

S1. The effect of the ^{1}H-SE on the ELDOR spectra and the origin of time dependence of A^{SE} parameter

As can be seen in also all ELDOR spectra, the influence of the ^{1}H-SE on the ELDOR spectra is significant and needs to be taken into account during the best-fit simulations using the eSD model for obtaining reliable Λ^{eSD} values. During the simulations the influence of the SE process on the EPR and ELDOR spectra is represented by an effective irradiation rate matrix in the polarization vector rate equation in Eq. 1. The effective strength of this fictitious irradiation is defined by introducing a SE parameter A^{SE}. In the main text it was shown that to achieve good fits to the ELDOR data obtained after different MW irradiation periods t_{MW} it was necessary to vary A^{SE}.

Population calculations

To obtain a better understanding of the SE effects on the spectra, we calculate first the SE influence in a small spin system by solving the rate equations for its populations introduced first in Ref. 1. For that purpose we consider a spin system consisting of nine coupled electrons, $n_e = 1,...,9$, and one nucleus, coupled to one of these electrons. As we have done in a recent publication we begin with a rotating frame Hamiltonian of the electron spins of the form[1]:

$$H_e = \sum_{n_e=1..9}\{(5-n_e)\delta\omega + \Delta\omega\}S_{n,z} + \sum_{n_e>n_e'} x_{n,n'}D(3S_{n_e,z}S_{n_e',z} - \bar{S}_{n_e}\cdot\bar{S}_{n_e'}) \qquad (1)$$

for equally spaced resonance frequencies of the electrons, $\delta\omega/2\pi = 10\,\mathrm{MHz}$. The mutual dipolar interactions between all electron pairs n_e and n_e' are determined by a set of randomly chosen constants $-1/2 < x_{n_e,n;_e} < 1$, with $\sum_{n_e<n_e'} x_{n_e,n_e'} = 0$ and an average dipolar strength D. The off-resonance value $\Delta\omega$ determined by the MW frequency is measured with respect to ω_e, the Larmor frequency of $n_e = 5$. The nucleus is coupled to $n_e = 2$ and extends the H_e Hamiltonian by the hyperfine interaction term

$$H_{e-n} = A_2 2S_{2,z}I_z + 0.5(A_2^+S_{2,z}I^+ - A_2^-S_{2,z}I^-) \qquad (2)$$

In this way, we can construct a matrix representation of the sum Hamiltonian $H_e + H_{e-n}$ in the manifold of electron and nuclear product states determined by S_z and I_z. After diagonalization we can describe the spin system by its eigenstate populations $p_i^{M_e}(t)$, ignoring fast-decaying coherences generated by the MW irradiation, and solve the rate equation for the vector composed of all these populations[1] $\bar{p}(t)$:

$$\frac{d}{dt}\bar{p}(t) = -(\mathbf{R}_{1e} + \mathbf{R}_{1n} + \mathbf{R}_{D} - \mathbf{W}_{MW})\bar{p}(t) \qquad (3)$$

Here $\mathbf{R}_{1e}$ and $\mathbf{R}_{1n}$ are the electron and nuclear spin-lattice relaxation rate matrices, respectively, $\mathbf{W}_{MW}$ is the MW rate matrix and $\mathbf{R}_{D}$ is the cross relaxation rate matrix. The elements of these matrices are defined in Ref. 1. Solving Eq. 3 for a set of dipolar and hyperfine interaction, relaxation and MW parameters we can follow, for example, the time evolution of $\bar{p}(t)$ for different irradiation times t_{MW} and from its elements and we can calculate EPR line shapes $E_{sim}^{EPR}(\Delta\nu_{det},[t_{MW},\Delta\nu_{exc}])$ for fixed t_{MW} and $\Delta\nu_{exc}$ values. By normalizing them with respect to the equilibrium EPR line shape $E_{eq}^{EPR}(\Delta\nu_{det})$ we can plot normalized EPR profiles

$$\mathrm{E}_{sim}^{EPR}(\Delta\nu_{det},[t_{MW},\Delta\nu_{exc}]) = \frac{E_{sim}^{EPR}(\Delta\nu_{det},[t_{MW},\Delta\nu_{exc}])}{E_{eq}^{EPR}(\Delta\nu_{det})} \qquad (4)$$

These normalized EPR spectra for a set of MW frequencies, $\Delta\nu_{exc}$ values, can also be presented as ELDOR profiles, $\mathrm{E}_{sim}^{ELDOR}(\Delta\nu_{exc},[t_{MW},\Delta\nu_{det}])$. In addition we can evaluate the NMR signal of the single nucleus.

Before showing some results of the 10-spin system we first consider a two-spin system $\{n-e\}$. Choosing the following parameters,

$$\begin{aligned} &T_{1e} = 50\,\mathrm{ms},\ T_{2e} = 100\,\mu\mathrm{s},\ T_{1n} = 1\mathrm{s}, \\ &T_{D} = 0.1\mathrm{ms},\ \nu_{1} = 0.05\,\mathrm{MHz},\ \nu_{n} = 65\,\mathrm{MHz}, \\ &D/2\pi = 2\mathrm{MHz},\ A_{2}/2\pi = -1\mathrm{MHz}, A_{2}^{\pm}/2\pi = 2\mathrm{MHz} \end{aligned} \qquad (5)$$

we can calculate ELDOR profiles. Choosing a nuclear Larmor frequency of 65MHz and setting the value of $\Delta\nu_{\mathrm{det}}$ at zero, we can plot the ELDOR spectrum $\mathrm{E}_{\mathrm{sim}}^{\mathrm{ELDOR}}(\Delta\nu_{\mathrm{exc}},[\Delta\nu_{\mathrm{det}}])$ and the DNP spectrum $\mathrm{E}_{\mathrm{sim}}^{\mathrm{n}}(\Delta\nu_{\mathrm{exc}})$

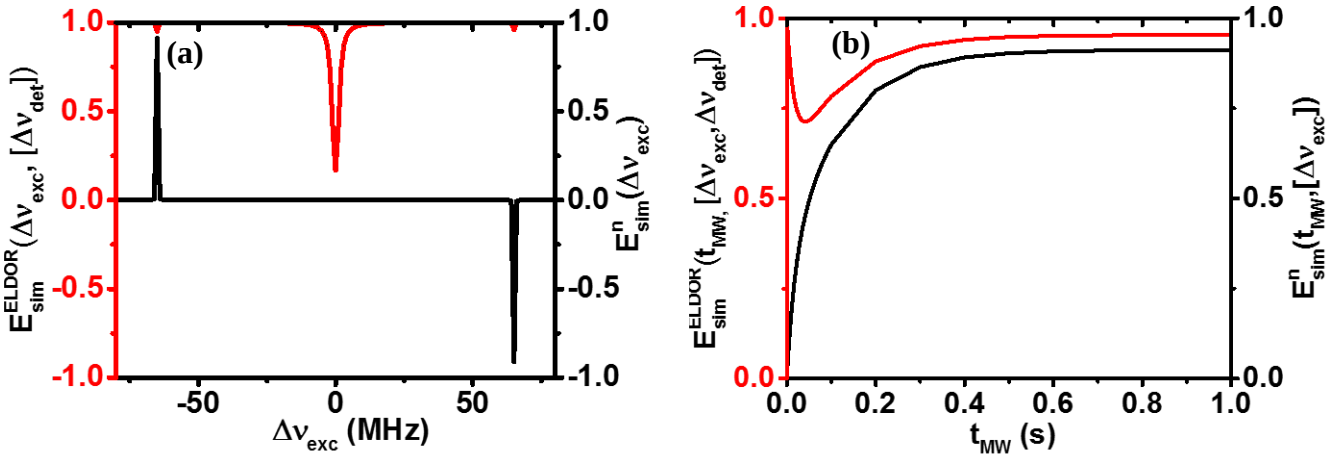

Figure S7. (a) The steady-state ELDOR profile $\mathrm{E}_{\mathrm{sim}}^{\mathrm{ELDOR}}(\Delta\nu_{\mathrm{exc}},[\Delta\nu_{\mathrm{det}}])$ for $\Delta\nu_{\mathrm{det}}=0$ in red and steady-state DNP spectrum, $\mathrm{E}_{\mathrm{sim}}^{\mathrm{n}}(\Delta\nu_{\mathrm{exc}})$ in black are shown for a hyperfine-coupled system of 1 electron and 1 nucleus with Larmor frequencies $\nu_n=65\,\mathrm{MHz}$. (b) For the same two-spin system, the polarization of the electron (in red), nucleus (in black) are calculated as function of MW irradiation time with $\nu_1=0.05\,\mathrm{MHz}$, while the position of the MW is at the nuclear Larmour frequency, $\Delta\nu_{exc}=-65\mathrm{MHz}$. In each case, the normalization is done with respect to the electron polarization at thermal equilibrium.

as a function of the MW frequency $\Delta\nu_{exc}$. For a long t_{MW} value we show in Fig. S7a both of these spectra. As expected we observe a positive-negative signal profile for the nucleus with extrema at the transition frequencies of the zero and double quantum transitions $\Delta\nu_{\mathrm{exc}}=\pm\nu_{\mathrm{n}}$, while the electron polarization gets slightly depleted at $\mathrm{E}_{\mathrm{sim}}^{\mathrm{ELDOR}}(\Delta\nu_{\mathrm{det}}\pm\nu_{\mathrm{n}},[\Delta\nu_{\mathrm{det}}])$. Following the nuclear and electron polarizations at $\Delta\nu_{\mathrm{exc}}=-\nu_{\mathrm{n}}$ as a function of t_{MW} in Fig. 7b we show that the nuclear polarization increases with a time scale equal to $T_{1\mathrm{e}}$ and the electronic polarization decreases very fast at the start and then returns towards a steady-state value $\mathrm{E}_{\mathrm{sim}}^{\mathrm{ELDOR}}(\Delta\nu_{\mathrm{exc}},\ [\Delta\nu_{\mathrm{det}}])<1$ also at a time scale of the $T_{1\mathrm{e}}$. Thus at this point, we conclude that the SE process can be detected by a depletion of the steady-state value of $\mathrm{E}_{\mathrm{sim}}^{\mathrm{ELDOR}}(\Delta\nu_{\mathrm{exc}},[\Delta\nu_{\mathrm{det}}])$ at $\Delta\nu_{exc}=\pm\nu_n$. We notice however that this value is not reached following a steady decaying function, but rather by an initial short decay followed by a partial recovery. The time evolution of the electron polarization due to the SE has already been observed experimentally[2]. In connection to our experimental

results discussed in section 3.2, this effect must be accounted for by changing A^{SE} with irradiation time in our simulations of t_{MW} dependent spectra.

We now return to the 10-spin system and explore the influence of the SE-DNP process on the electrons. We mention again that the nucleus is coupled to the electron $n_e = 2$. In this case, it is interesting to calculate the t_{MW} dependent ELDOR profiles for $\Delta\nu_{det} = \Delta\nu_2$. We realize that in the present system in addition to the SE-DNP mechanism the system is also exposed to the electron dipolar interactions and the cross relaxation mechanism, which can both diminish the effect of the SE on the electron depolarizations. It is therefore expected that the influence of the SE-DNP process is more pronounced when the electron coupled to the nucleus has a relatively small dipolar interaction with its neighboring electrons. Therefore in our calculations, after choosing a set of random $x_{n_e,n_e'}$ values for the electron-electron dipolar interaction we reduce all values with $n_e = 2$ or $n_e' = 2$ by a factor of three. The parameters in Eq. (5) are also chosen for the 10-spin system and by solving Eq. (3) we obtained the ELDOR profiles $E_{sim}^{ELDOR}(\Delta\nu_{exc},[t_{MW}],[\Delta\nu_2])$ shown in Fig. S8a for varying t_{MW} and $\Delta\nu_{exc}$. We clearly see the effect of the SE on the electrons for the ZQ case $\Delta\nu_{exc} = \Delta\nu_2 - \nu_n$ which is positioned outside the EPR spectrum and for the DQ case $\Delta\nu_{exc} = \Delta\nu_2 + \nu_n = \Delta\nu_8$ which is inside the EPR spectrum. Careful observation shows in Fig8a that initially, the "inside" SE electron depletions are strong and that they disappear for large t_{MW} values due to the cross-relaxation broadening. To verify the influence of the dipolar interaction on the SE depolarization, we repeated the ELDOR calculation for $t_{MW} = 5\,\mathrm{ms}$ without reducing the $x_{n_e,n_e'}$ values for the electron $n_e = 2$ and observe as expected that the SE influence is significantly reduced (not shown).

S2. Bin-polarization calculations

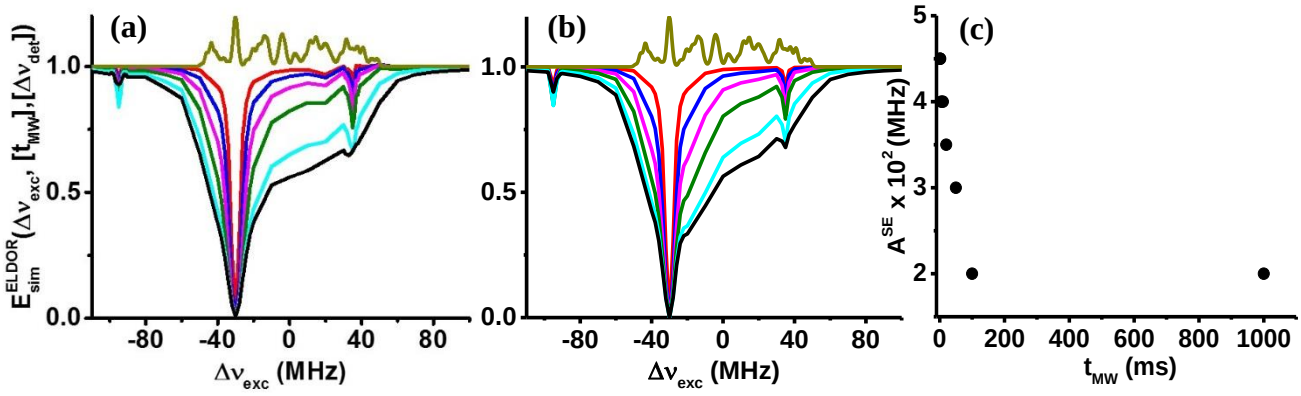

Figure S8. (a) The ELDOR $E_{sim}^{ELDOR}(\Delta\nu_{exc},[t_{MW}],[\Delta\nu_{det}])$ spectrum is calculated for a coupled spin system of 9 electrons and 1 nucleus for $t_{MW}=2,5,10,20,50$ and 10^3 ms which are plotted in red, blue, magenta, green, cyan, black, respectively. The corresponding EPR spectrum is shown on top of the ELDOR profiles. (b) The ELDOR $E_{sim}^{ELDOR}(\Delta\nu_{exc},[t_{MW}],[\Delta\nu_{det}])$ spectrum, calculated with eSD model for the same EPR spectra using $\Lambda^{eSD}=4\,\mu s^{-3}$, are shown with the same color coding. (c)The time dependence of A^{SE} used in the eSD simulations is shown.

At this point, we can try to reproduce the t_{MW}-dependent ELDOR profiles by using the eSD model[3] as described in Eq (1) in the main text. The elements of the SE matrix W_{SE}^{b} must be chosen such that the eSD model can reproduce similar ELDOR profiles presented in Fig 8a. The eSD derived ELDORs are presented in Fig. 8b.

In our previous work[3] to reproduce the steady-state profiles, we represented the SE as an effective on-resonance MW irradiation applied to the ZQ and DQ transitions of the electrons with a constant A^{SE} parameter. To continue in these lines but now also addressing the (decrease-increase) time dependence of the SE influence on the ELDOR spectra, we must allow this effective MW field at the position of solid effect to vary for each t_{MW} value. Thus the magnitudes of the matrix elements of W_{SE}^{b} in Eq. 1 (in the main text) for the calculation of $\bar{P}_e(t_{MW})$ vary for different t_{MW}'s:

$$\frac{d}{dt}P_{e,j}(t)=W_{SE,j}^{b}(t_{MW})P_{e,j}(t) \qquad (6a)$$

The actual values of these elements should be small and proportional to $\omega_1=2\pi\nu_1$ and we can write the diagonal elements of $W_{SE,j}^{b}(t_{MW})$ as:

$$W^{b}_{\mathrm{SE},j}(t_{\mathrm{MW}}) = \frac{\left(\{A^{\mathrm{SE}}_{j}(t_{\mathrm{MW}})/\omega_{\mathrm{n}}\}\omega_1\right)^2 T_{2\mathrm{e}}}{1+(\Delta\omega'_{\mathrm{exc}}-(\omega_j-\omega'_{\mathrm{n}}))^2 T^2_{2\mathrm{e}}} + \frac{\left(\{A^{\mathrm{SE}}_{j}(t_{\mathrm{MW}})/\omega_{\mathrm{n}}\}\omega_1\right)^2 T_{2\mathrm{e}}}{1+(\Delta\omega'_{\mathrm{exc}}-(\omega_j+\omega'_{\mathrm{n}}))^2 T^2_{2\mathrm{e}}} \qquad (6b)$$

where, because of the bin model, ω_{n}' is the bin frequency closest to the nuclear Larmor frequency and $\Delta\omega'_{\mathrm{exc}}$ the bin frequency closest to the actual excitation frequency[3]. The effective irradiation strength in this representation of the SE is of the form $\{A^{\mathrm{SE}}_{j}(t_{\mathrm{MW}})/\omega_{\mathrm{n}}\}\omega_1$. Here we can assume that the $A^{\mathrm{SE}}_{j}(t_{\mathrm{MW}})$ parameters are of the order of magnitude of $A^{\pm}$, the strength of some average pseudo-hyperfine coefficient of the electron-nuclear interaction. In the present example, only the electron $n_{\mathrm{e}}=2$ has a nuclear neighbor and therefore for all j $A^{\mathrm{SE}}_{j}=0$ except $A^{\mathrm{SE}}_{2}\neq 0$. Consequently, we report here only the ELDOR profile for $\omega_{\mathrm{det}}=\omega_2$. In Fig. S8(b) we show the fitting of the ELDOR profile with the eSD model, where we used for each t_{MW} a different $A^{\mathrm{SE}}_{2}(t_{\mathrm{MW}})$ coefficient. Without modifying the value of $A^{\mathrm{SE}}_{2}(t_{\mathrm{MW}})$ we could not fit the ELDOR spectra.

S3. On the explanation of experimentally obtained *c* dependence of Λ^{eSD}

In order to demonstrate the parametric dependence of Λ^{eSD} on D we have calculated steady state EPR spectra, $E_{sim}^{EPR}(\Delta\nu_{det},[\Delta\nu_{exc}])$, for $D/2\pi = 1.5, 2, 2.5$ and 3 MHz using the same spin system. The other parameters are kept same as mentioned in Eq. 5 except $T_D = 0.16, 0.1, 0.06$ and 0.04 ms. This square dependence of T_D on D enhances the D- dependence of the depolarization induced by both the state mixing due to the dipolar interaction itself and the cross-relaxation process[3]. In Fig.S9 a-d we show the steady state EPR spectra during MW irradiation and the equilibrium EPR spectra, respectively in red and green, for different D values. The reduction of the amplitudes of the red spectra is to a large extend a result of the shortening of T_D. An effect to reproduce the steady state spectra using the eSD model and determining some Λ^{eSD} value for each D value is shown in black in Fig. S9 a-d. The fittings show that the eSD model succeeds to reproduce the amplitudes and the main features of the steady state spectra reasonably well. The accuracy of the Λ^{eSD} values, determined by χ^2 minimization, is of the order of ten percent. In Fig. S10 we plot the Λ^{eSD}'s as a function of D and fitted an power function through the values of the form $\Lambda^{eSD} = \lambda D^{\ell}$, with Λ^{eSD} in units of μs^{-3} and D in MHz. The result of this fitting procedure is $\ell = 3.5 \pm 0.5$. This strong dependence is for this set of spin systems a mainly a result of the modification in T_D and the fact that T_{1e} was not modified, where in experimental cases T_{1e} changes with concentration. We should therefore expect that in practice we should power values much smaller than 3.5.

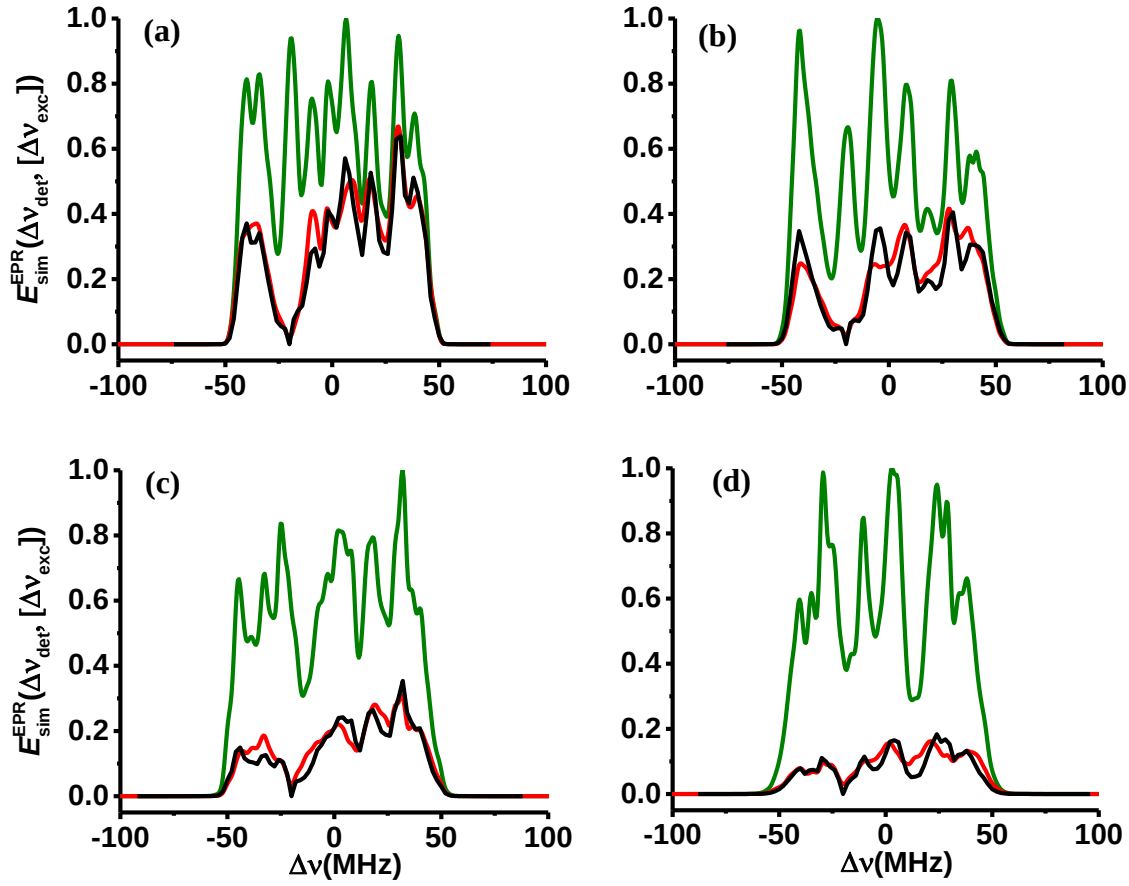

Figure S9. The steady-state EPR, $E_{\mathrm{sim}}^{\mathrm{EPR}}(\Delta\nu_{\mathrm{det}},[\Delta\nu_{\mathrm{exc}}])$ spectrum (Red) and the equilibrium EPR (Green) is calculated for a coupled spin system of 9 electrons (without the nucleus) for $D/2\pi = 1.5, 2, 2.5$ and 3 MHz, are shown in a-d in the same order. The steady-state EPR are fitted with the eSD model (Black) with $\Lambda^{\mathrm{eSD}} = 3, 9, 16$ and $35\,\mu s^{-3}$ in the same order.

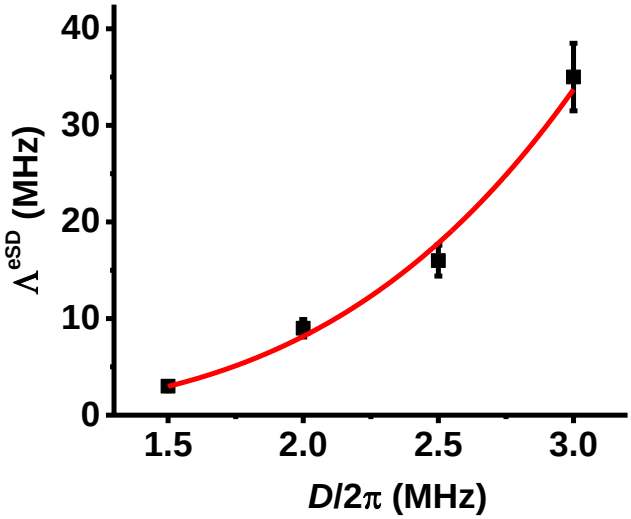

Figure S10. The average dipolar strength, *D*, dependence of Λ^{eSD} derived from the comparison of model spin calculation and the eSD rate equation on EPR spectra of $D/2\pi = 1.5, 2, 2.5$ and 3 MHz. The solid black line is the best fitted curve for a function of the form $\Lambda^{eSD} = \kappa D^{\gamma}$ with $\gamma = 3.5 \pm 0.5$.

References

1 K. Kundu, A. Feintuch and S. Vega, Electron–Electron Cross-Relaxation and Spectral Diffusion during Dynamic Nuclear Polarization Experiments on Solids, *J. Phys. Chem. Lett.*, 2018, **9**, 1793–1802.

2 V. Nagarajan, Y. Hovav, A. Feintuch, S. Vega and D. Goldfarb, EPR detected polarization transfer between Gd3+and protons at low temperature and 3.3 T: The first step of dynamic nuclear polarization, *J. Chem. Phys.*, 2010, **132**, 214504.

3 Y. Hovav, I. Kaminker, D. Shimon, A. Feintuch, D. Goldfarb and S. Vega, The electron depolarization during dynamic nuclear polarization: measurements and simulations, *Phys. Chem. Chem. Phys.*, 2015, **17**, 226–244.